ADVANCED MATERIALS
www.advmat.de

Ultrathin Magnetic 2D Single-Crystal CrSe

*Yu Zhang, Junwei Chu, Lei Yin, Tofik Ahmed Shifa, Zhongzhou Cheng, Ruiqing Cheng, Feng Wang, Yao Wen, Xueying Zhan, Zhenxing Wang, and Jun He**

2D magnetic materials have generated an enormous amount of attention due to their unique 2D-limited magnetism and their potential applications in spintronic devices. Recently, most of this research has focused on 2D van der Waals layered magnetic materials exfoliated from the bulk with random size and thicknesses. Controllable growth of these materials is still a great challenge. In contrast, 2D nonlayered magnetic materials have rarely been investigated, not especially regarding their preparation. Cr_nX (X = S, Se and Te; $0 < n < 1$), a class of nonlayered transition metal dichalcogenides, has rapidly attracted extensive attention due to its abundance of structural compounds and unique magnetic properties. Herein, the controlled synthesis of ultrathin CrSe crystals, with grain size reaching the sub-millimeter scale, on mica substrates via an ambient pressure chemical vapor deposition (CVD) method is demonstrated. A continuous CrSe film can also be achieved via precise control of the key growth parameters. Importantly, the CVD-grown 2D CrSe crystals possess obvious ferromagnetic properties at temperatures below 280 K, which has not been observed experimentally before. This work broadens the scope of the CVD growth of 2D magnetic materials and highlights their significant application possibilities in spintronics.

Recently, the extensive amount of investigations into 2D materials, such as MoS_2,[1–4] WS_2,[5,6] $MoTe_2$,[7] and $NbSe_2$,[8] has revealed a wide range of intriguing electronic phenomena and performance, which is attributed to their unique structures and excellent physical properties resulting from their reduced dimensionality.[9–11] Among these compounds, 2D magnetic materials have rarely been reported in recent years.[12–16] The ability to control spin orientations makes 2D magnets an excellent candidate for the development of spintronic logic and memory devices. These magnetic materials provide extraordinary opportunity to study intrinsic magnetic and physical phenomena at the nanometer scale without introducing any additional magnetic dopants.[17] In particular, the very recent discovery of magnetic long-range order in 2D van der Waals (vdW) materials[18–21] opens the door for fundamental physics research and device applications, which is a substantial breakthrough and has attracted much attention.

Very recently, several experiments focusing on the intrinsic and extrinsic magnetism of 2D materials have been conducted. Ferromagnetic behavior has occurred at exfoliated 2D van der Waals magnetic semiconductors, such as Fe_3GeTe_2,[22] $CrGeTe_3$,[14] and CrI_3.[23,24] For example, Fe_3GeTe_2[21] was shown to exhibit robust 2D ferromagnetism with strong perpendicular anisotropy when reduced down to monolayer thickness. Its Curie temperature (T_c) showed various layer-number-dependent magnetic phenomena. Interestingly, introducing an ionic gate raised the T_c to room temperature, much higher than the T_c of the bulk material, which was a great breakthrough. Afterward, van der Waals heterostructures formed by an ultrathin ferromagnetic semiconducting CrI_3 and monolayered WSe_2 have been created and exhibited unprecedented control of the spin and valley pseudospin, which indicated their important potential in spin and valleytronics.[23] However, most of these magnetic 2D materials are unstable in the air, which impedes research into their intrinsic magnetism and practical applications. Hence, exploiting new magnetic materials is a major challenge. Nonlayered 2D materials are good candidates due to their abundance of material systems and structures, which exhibit outstanding performance.[25,26] However, among these materials, 2D nonlayered magnetic materials have yet to be explored. In addition, recently reported 2D magnetic materials have mostly been layered structures stacked by weak vdW interactions, which leads to their being easily exfoliated into few-layered or monolayered structures from the bulk. However, the exfoliation method is time-consuming, affords little control over the thickness and domain size, and is incompatible with batch production. The exfoliation method is not suitable for the synthesis of 2D nonlayered materials due to its strong chemical bonds. Recently, the chemical vapor deposition (CVD) method has

Dr. Y. Zhang, L. Yin, Dr. T. A. Shifa, Z. Cheng, R. Cheng, Dr. F. Wang, Y. Wen, X. Zhan, Prof. Z. Wang, Prof. J. He
CAS Center for Excellence in Nanoscience
CAS Key Laboratory of Nanosystem and Hierarchical Fabrication
National Center for Nanoscience and Technology
Beijing 100190, China
E-mail: hej@nanoctr.cn

J. Chu
State Key Laboratory of Electronic Thin Films and Integrated Devices
University of Electronic Science and Technology of China
Chengdu 610054, China

L. Yin, R. Cheng, Y. Wen, Prof. Z. Wang, Prof. J. He
Center of Materials Science and Optoelectronics Engineering
University of Chinese Academy of Science
Beijing 100049, China

The ORCID identification number(s) for the author(s) of this article can be found under https://doi.org/10.1002/adma.201900056.

DOI: 10.1002/adma.201900056

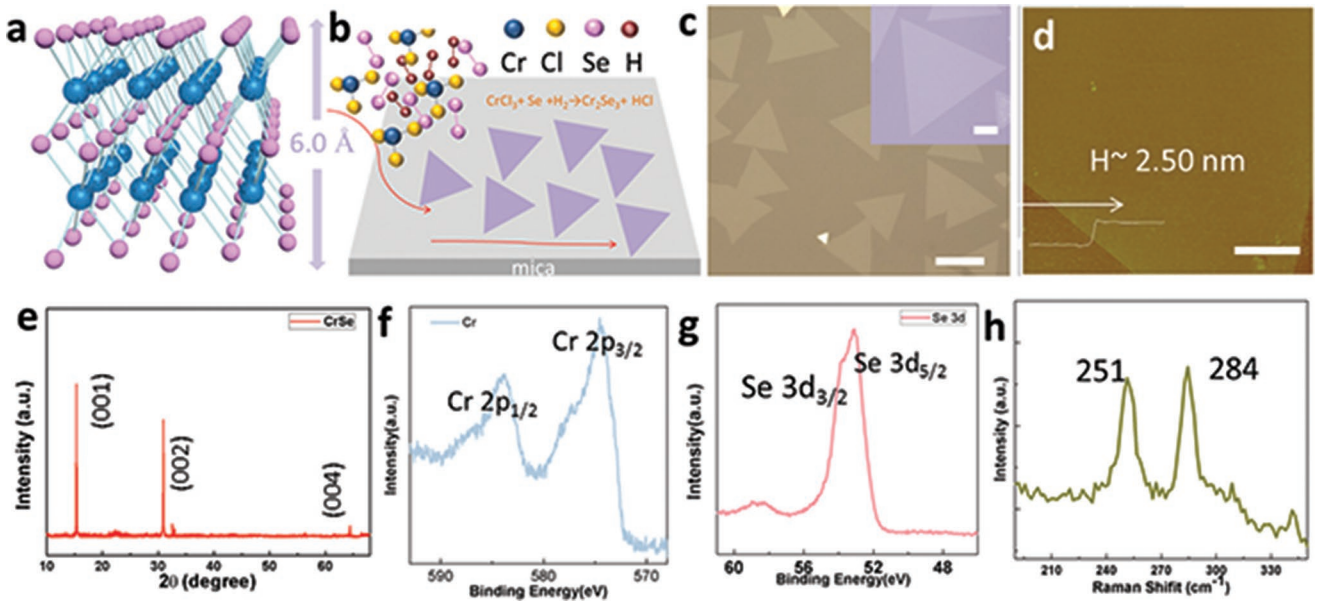

Figure 1. APCVD synthesis of the CrSe crystals and characterizations. a) Structural model of the CrSe crystal. b) Schematic view of the related reaction process. c) OM image of uniform CrSe crystals grown on the mica substrate. The inset shows an ultrathin CrSe crystal with an edge length of 0.15 mm. Scale bar, 25 µm. d) AFM image and its corresponding height profile for a triangular CrSe crystal, which shows a typical thickness of ≈2.5 nm. Scale bar: 1 µm. e) XRD profile for the CrSe flakes on SiO_2/Si. f) XPS characterization of Cr 2p peaks of the as-grown CrSe on mica. g) XPS characterization of the Se 2p peaks of the as-grown CrSe on mica. h) Typical Raman spectrum of CrSe on SiO_2/Si.

been considered a swift and effective approach for the synthesis of various 2D atomic crystals, such as metallic graphene,[27] insulating h-BN,[28] and semiconducting MoS_2.[29] However, obtaining 2D magnetic materials via the CVD method remains a great challenge. Recent research has mainly focused on 2D vdW magnetic materials, the variety for which is limited. In contrast, 2D nonlayered materials, which have an abundance of structures, have hardly been studied, providing a huge challenge for expanding the available magnetic materials systems and studying 2D-limited magnetism.

Cr_nX (X = S, Se and Te; $0 < n < 1$), a new class of nonlayered Cr-based chalcogenides, has been explored and has received tremendous attention due to its magnetic properties. For example, Cr_2S_3 is a ferrimagnetic semiconductor with Néel temperature of $T_N \approx 120$ K.[30] Cr_2Te_3 crystallizes in a NiAs-type structure and has been proven to be a ferromagnet, for which the Curie temperature is ≈200 K.[31] Other compounds, such as CrTe, $Cr_{0.62}Te$, and Cr_5Te_8, also exhibit obvious ferromagnetic properties.[32–34] Additionally, Cr_nX (X = S, Se and Te; $0 < n < 1$) possesses a number of binary compounds with different component ratios, which leads to a number of structural phases and physical properties.[35–39] The Cr_nSe obtained thus far has mainly been in bulk state and few properties have been reported for its 2D structure. Besides, it is suspected that CrSe crystals have anomalous magnetic properties, but few works have been reported on CrSe, not to mention the synthesis of 2D CrSe crystals. Herein, we have exploited vdW epitaxy to controllably synthesize ultrathin nonlayered CrSe crystals on mica substrates via an ambient pressure chemical vapor deposition (APCVD) approach. Optical microscopy (OM) and atomic force microscopy (AFM) studies revealed that the synthesized CrSe flakes exhibit triangular shapes with a lateral size of up to 150 µm and thicknesses as thin as 2.5 nm. By controlling the growth time and source–substrate distance, the key factors in the CVD growth process, high-quality and large-size CrSe flakes can be synthesized. A continuous CrSe film was obtained via precise control of the growth parameters. Interestingly, we have characterized the ferromagnetic properties of CVD-grown CrSe flakes for the first time, which paves the way for further studies on these magnetic materials and magnetism-related applications in spintronics.

The ground state of CrSe crystallizes into space group *P63/mmc(194)* with the lattice parameters a = 3.61 Å, b = 3.61 Å, and c = 5.78 Å, which are described by the X-ray diffraction (XRD) standard card (PDF#02-0883). **Figure 1**a depicts the crystal structure of nonlayered CrSe, which shows that the unit cell of CrSe has a Se-Cr-Se-Cr-Se quintuple layered structure. This structure can be considered to be two $CrSe_2$ layers stacked together by sharing a layer of Se atoms. The top view and side view of the CrSe crystal structure are provided in Figure S1 (Supporting Information). The thickness of the unit cell between the top and bottom CrSe layer is ≈0.6 nm. Figure 1b schematically illustrates the surface reaction that occurs during the epitaxial growth of CrSe crystals on freshly cleaved mica substrates via an APCVD system. More details on the growth process and experimental setup are provided in the Experimental Section and Figure S2 (Supporting Information). Briefly, chromium trichloride ($CrCl_3$) and selenium (Se) powders were used as reactants. Se powder, $CrCl_3$ mixed with a small amount of NaCl powder, and growth substrates (mica) were sequentially placed from the upstream to downstream, in a quartz tube. Notably, the use of NaCl powder, which has a low melting point, decreased the energy barrier and increase the growth rate, which has been discussed in previously reported

works.[6,40] During the APCVD process, an adequate amount of selenium vapor is conveyed downstream by a flow of 100 sccm Ar and 10 sccm H_2 and reacts with evaporated $CrCl_3$ at the rather high temperature of 735 °C. As a result, triangular CrSe flakes are successfully produced on the mica substrates, as seen in the OM in Figure 1c. Figure 1c shows the typical OM-observed morphologies of the as-grown CrSe triangles; the brightly contrasting flakes on the surface represent CrSe and the surrounding regions correspond to the mica substrates. All the CrSe crystals were triangularly shaped, which is in agreement with the crystal structure of CrSe. The maximum edge length of the CrSe domains was 150 µm, as confirmed by the inset in Figure 1c. Figure 1d shows a representative AFM image and demonstrates that the thickness can be as low as ≈2.5 nm, which is extremely thin for a non-layered material. In addition, the AFM image in Figure S3 (Supporting Information) gives a thickness of 0.6 nm for an occasional CrSe step edge, which is in good accordance with the thickness of the unit cell of the CrSe crystal. Further, XRD was employed to identify the crystal structure of as-grown samples. Notably, the XRD results were collected after transferring the sample on onto SiO_2/Si to eliminate the interference from mica substrates. As shown in Figure 1e, the XRD pattern of our CVD-grown sample is well matched to the (001) crystal planes of the standard hexagonal CrSe pattern (PDF#02-0883), which confirms the formation of CrSe crystals and their single-crystalline nature. Furthermore, the chemical states and elemental composition of the as-synthesized samples were determined by X-ray photoelectron spectroscopy (XPS; Figure 1f,g). It can be seen that the sample consists of Cr and Se atoms. The chemical states of Cr $2p_{1/2}$ and $2p_{3/2}$ can be identified from the peaks at binding energies of 584 and 574 eV (Figure 1f), whereas the peaks at 55 and 53 eV (Figure 1g) correspond to the $2p_{1/2}$ and $2p_{3/2}$ states of Se, respectively. Raman spectroscopy measurements were also performed on the CrSe sample that had been transferred onto SiO_2/Si to explore the intrinsic optical properties of a newly synthesized material. Figure 1h shows the two characteristic Raman peaks at 251 and 284 cm^{-1} (under 514 nm laser excitation), and layer-thickness-dependent Raman spectra are provided in Figure S4 (Supporting Information). Additionally, the time-dependent Raman spectra also emphasize the stability of our CVD-grown CrSe samples in air, as shown in Figure S5 (Supporting Information). In brief, these results reveal that large-scale ultrathin CrSe crystals were epitaxially grown on mica through an APCVD method.

To optimize the growth results, detailed systematic studies were conducted to investigate the effect of growth time and source–substrate distance (D_{ss}) on the growth results (**Figure 2**). With the other growth parameters (growth temperature, carrier gas, and D_{ss}) remaining constant, the CrSe nanosheets

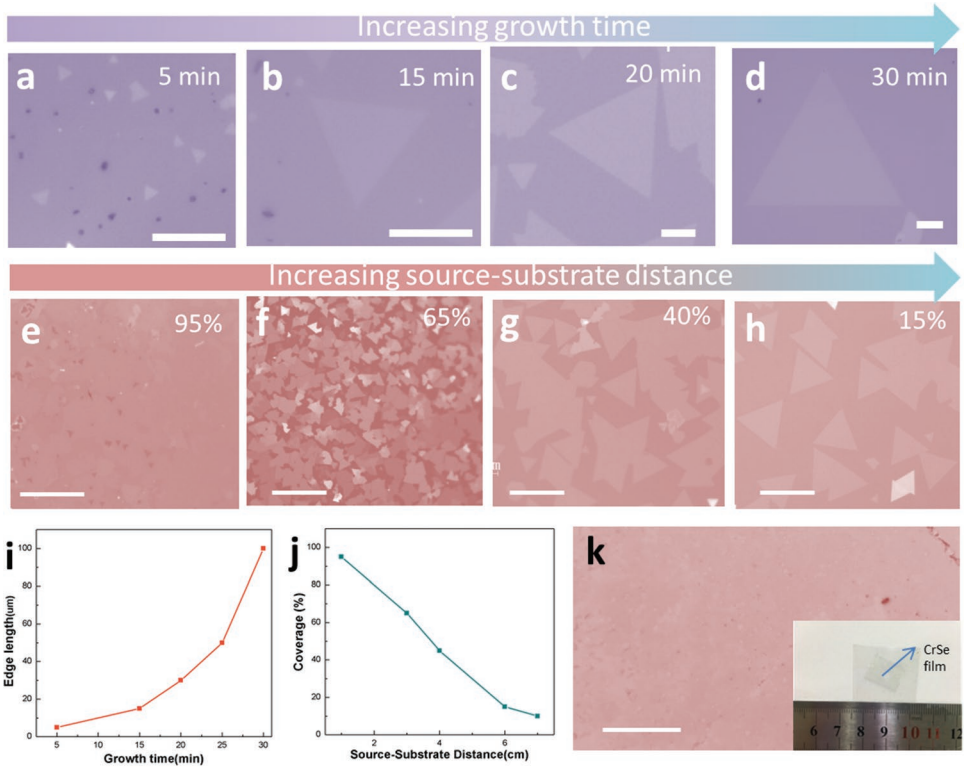

Figure 2. Typical OM images of CrSe crystals grown under different conditions. a–d) Growth-time dependent OM images of as-grown CrSe flakes, which were synthesized under the same conditions (grown at 735 °C), on mica with different domain sizes of 5, 15, 50, and 100 µm for the different growth times of 5 min (a), 15 min (b), 20 min (c), and 30 min (d), respectively. Scale bar: 10 µm. e–h) D_{ss}-dependent OM images of as-grown CrSe flakes on mica, which were synthesized under the same conditions (grown at 735 °C), with coverage of ≈95%, 65%, 40%, and 10% for the different D_{ss} of ≈1 cm (e), 4 cm (f), 6 cm (g), and 7 cm (h), respectively. Scale bar: 25 µm. i) CrSe edge length as a function of the growth time. j) CrSe coverage on mica as a function of the D_{ss}. k) Typical OM image of a continuous CrSe film on mica substrate with a photograph of a CrSe film transferred onto flexible PET as inset.

synthesized at different growth times exhibit an obvious change in their domain size. Typical OM images of CrSe grown on mica different lengths of time are presented in Figure 2a–d. Under proper growth conditions, the domain size of the CrSe triangles increases from 5 to 100 μm with increasing growth time from 5 to 30 min. Briefly, when there is a suitable nucleation density on growth substrates, the domain size of the CrSe flakes can be efficiently increased, until joining together to form a film, by providing a continuous and sufficient amount of the reactants. These results clearly show that the growth time critically affects the crystal size. In addition, a change from very small domain size to large domain size with increasing growth time is observed (Figure 2i). Furthermore, in the same growth batch, the distance between the $CrCl_3$ source and the mica substrates (D_{ss}) was also found to be an essential parameter for determining the growth results. It is expected that the concentration of available $CrCl_3$ will decrease with increasing D_{ss}, leading to different coverage of the CrSe flakes on the mica substrates. As a consequence, the coverage of CrSe on the mica substrates can be effectively tuned from 95% to 15% for the different D_{ss} (1, 3, 4, 6, and 7 cm), as shown in the representative OM images of the as-grown CrSe flakes on mica (Figure 2e–h). In summary, $CrCl_3$ powder is placed upstream, as a growth precursor, and transported downstream by carrier gas. Then the evaporated $CrCl_3$ has a distinct concentration gradient with increasing distance, which ultimately leads to different nucleation densities between upstream and downstream locations. Obviously, the nucleation density and domain size are very sensitive to the precursor concentration. Figure 2e shows a nearly continuous CrSe film that formed when $D_{ss} \approx 1$ cm due to the high nucleation density, which is in contrast with the discrete triangles that formed when $D_{ss} \approx 7$ cm (Figure 2h) due to the low nucleation density. At the same time, another trend for increasing D_{ss} can be observed. As shown in Figure 2e–h, the domain sizes of the CrSe crystals become larger with increasing D_{ss}. The reason is that a low nucleation density is beneficial for achieving a large domain size at the proper growth time and growth temperature. A similar change from a high degree of substrate coverage to a small degree of substrate coverage is observed with increasing growth D_{ss}, as shown in Figure 2j. These growth trends are in good accordance with those seen in the synthesis of layered WS_2 via the CVD method.[41,42] In this regard, through appropriate control of the growth time and D_{ss}, near-complete high-quality and large-scale CrSe films can be obtained directly on mica via a facile APCVD method. As shown in Figure 2k, a typical OM image of the sample surface shows a highly uniform color contrast, indicating the formation of an in-plane CrSe film. This atomic thin film layer can also be transferred onto flexible poly(ethylene terephthalate) (PET) substrates (inset photograph in Figure 2k), which shows its potential application in the field of flexible electronic/optoelectronic devices.

Further, high-resolution transmission electron microscopy (HRTEM) was employed to investigate the detailed atomic structure and crystallinity of the CVD-grown CrSe samples. The as-grown CrSe triangles on the mica substrate were first transferred onto carbon-supported Cu grids via a poly(methyl methacrylate) (PMMA) assisted transfer method[43] and then characterized by TEM. The low-magnification TEM image (**Figure 3**a) shows a typical triangular CrSe flake on the Cu grids, indicating the material remained intact during transfer. Further, Figure 3b shows an HRTEM image of the perfect hexagonal arrangement of the atoms. The (110) lattice plane spacing (d_{110}) measured from Figure 3b is ≈0.181 nm, which is in good accordance with that calculated from the standard XRD results (PDF#02-0883). The corresponding selective area electron diffraction (SAED) pattern (Figure 3c) confirms the excellent single-crystal nature of the CrSe triangles as indicated by only one set of hexagonal diffraction spots being present. Based on the SAED results, we can calculate the (110) lattice plane spacing of CrSe to be 0.181 nm, which is consistent with the spacing observed from the HRTEM image. Further

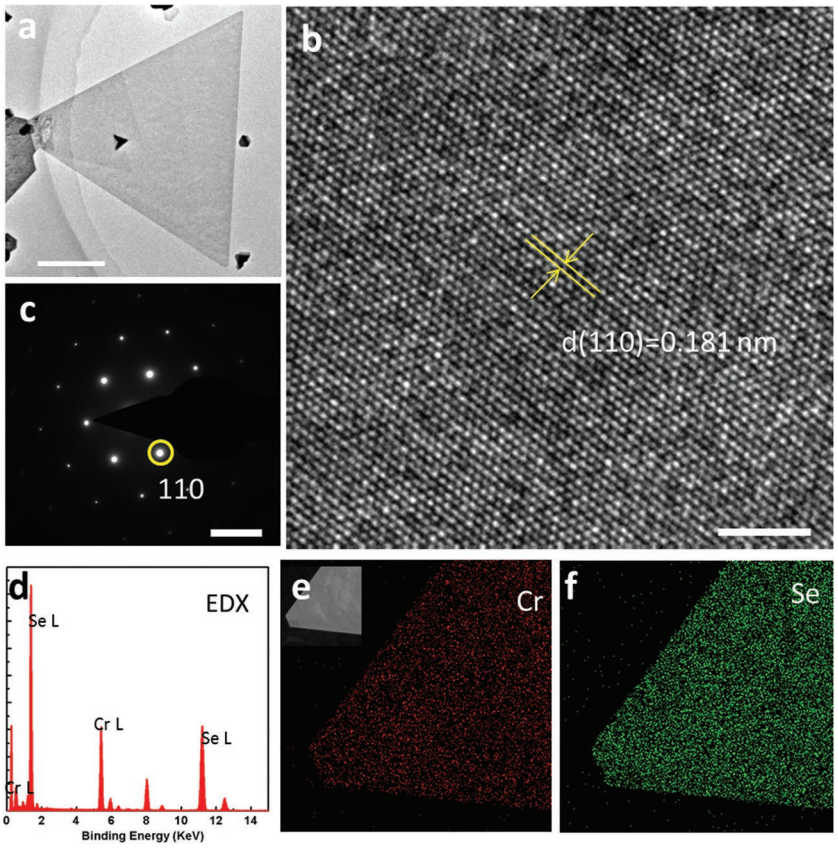

Figure 3. Atomic structural characterized by high-resolution transmission electron microscopy (HRTEM). a) Low-magnification TEM image of a triangular CrSe flake. Scar bar: 1 μm. b) High-resolution TEM image of a CrSe crystal. Scale bar: 2 nm. c) Corresponding SAED pattern captured within a 500×500 nm^2 area. Scar bar: 5 nm^{-1}. d) EDS elemental analysis of a CrSe flake on a TEM grid. e,f) EDS mapping images of Cr and Se in the corner of a CrSe triangle on a TEM grid. The inset of (e) is the TEM image of the selected area.

energy-dispersive spectroscopy (EDS) elemental mapping was utilized to analyze the elemental composition of the synthesized CrSe crystals. Figure 3d shows that our CVD-synthesized samples consist of Cr and Se atoms. The EDS maps (Figure 3e,f) present the spatial distribution of the Cr and Se atoms in the corner region of a triangle, which indicates the formation of CrSe crystals and its compositional uniformity as reflected by the uniform color distribution. Together, these TEM results confirm the achievement of ultrathin single-crystal CrSe flakes and demonstrate their highly crystalline nature, which ensures a good material foundation for further research and applications.

It is expected that these CrSe crystals, as a typical member of the Cr_nX class of materials, are likely to possess distinct magnetic properties. Thus, to verify our prediction and study the magnetic properties of the synthesized CrSe crystals, a physical property measurement system (PPMS) was utilized on the CrSe samples that had been transferred onto SiO_2/Si. Because of the very high diamagnetic background signal and potential residual signal from mica, all CrSe samples were transferred onto SiO_2/Si substrates before the magnetic test. Subsequently, the magnetic response of the different CrSe samples to parallel and vertical magnetic field was both investigated, as shown in **Figure 4** and Figure S6 (Supporting Information). In addition, the morphologies and thickness distributions of the samples are provided in Figure S7 (Supporting Information). First, a field cooling process was conducted under an external field of 1000 Oe. The temperature-dependent magnetic moments (M–T) were measured and are shown in Figure 4a,c, which indicates the obvious ferromagnetic nature of our CVD-grown CrSe samples. As shown in Figure 4a, when the temperature is just below 280 K, the spontaneous magnetization of the CrSe lattice exceeds the thermal fluctuation induced net magnetic moment. Thus, the magnetic moment reaches a saturation state with decreased temperature. Additionally, when applying a vertical magnetic field, the temperature-dependent magnetic moment shows a similar tendency. In contrast, the saturated moment under a vertical magnetic field is ≈100 μemu, which is much higher than that under a parallel magnetic field, as shown in Figure 4a. These data indicate that the out-of-plane CrSe crystals possess a much higher magnetic susceptibility than that of the in-plane crystals. Importantly, a transition from the paramagnetic state to the ferromagnetic state occurs at ≈280 K. Further, the magnet field dependent moments are also obtained and shown in Figure 4b,d. Figure 4b shows the magnetic hysteresis curves acquired at different temperatures ranging from 300 to 5 K under a parallel magnetic field, while Figure 4d displays the magnetic hysteresis curves acquired at different temperatures under a vertical magnetic field. The results demonstrate obvious magnetic hysteresis when the

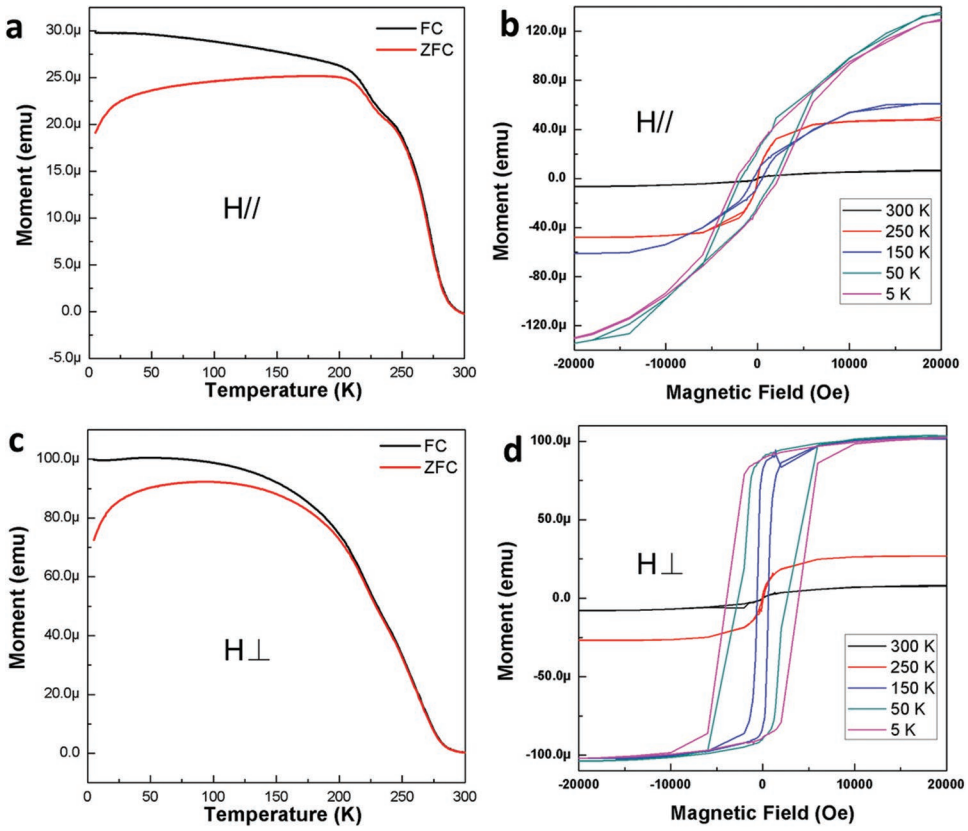

Figure 4. Magnetic characterization of CrSe samples on SiO_2/Si. a) Temperature-dependent magnetization of CrSe flakes transferred onto a SiO_2/Si substrate with a parallel magnetic field at 1000 Oe. b) Magnetic hysteresis loops obtained at different temperature for the CrSe flakes with a parallel magnetic field. c) Temperature-dependent magnetization of CrSe flakes transferred on a SiO_2/Si substrate with a vertical magnetic field at 1000 Oe. d) Magnetic hysteresis loops acquired at different temperature for CrSe with a vertical magnetic field.

temperature is below 280 K, regardless of whether a parallel field (Figure 4b) or a vertical field (Figure 4d) is applied. A mall magnetic hysteresis exists at 250 K, a magnified view of which is shown in Figure S8 (Supporting Information). Hence, there is a transition from the paramagnetic state to the ferromagnetic state with decreasing temperature, which is in good accordance with the *M*–*T* results. Moreover, the hysteresis in Figure 4d is much stronger than that in Figure 4b, which again confirms the higher magnetic susceptibility for the out-of-plane CrSe crystals. These results demonstrate that our CVD-grown CrSe crystals exhibit obvious ferromagnetic properties, which possess significant importance for the investigation of magnetism and magnetism-related applications.

To further investigate the electronic properties and magnetism-related properties of the CVD-grown CrSe crystals, four-terminal electronic devices were fabricated on the CrSe crystals after they had been transferred onto SiO_2/Si. The inset of **Figure 5**a shows a typical OM image of a device constructed on a single crystal CrSe triangle with a thickness of 5.1 nm (shown in Figure S9, Supporting Information). Figure 5a demonstrates a linear I_{ds}–V_{ds} curve collected at room temperature, indicating ohmic contact between CrSe and the electrodes (Figure S10, Supporting Information). Figure 5b shows the temperature-dependent resistivity of the CrSe device, which exhibits an increase in the resistance from 300 to 264 K and then an obvious decrease in the resistance from 264 to 50 K. The resistivity of the CrSe-based device is comparable to that of previously reported 2D materials.[44,45] The saturation at ≈264 K is considered to be induced by the magnetic phase transition, for which the result is well matched with the above *M*–*T* results (Figure 4). Moreover, Figure 5c,d presents the magnet field-dependent resistance of the CrSe-based devices at 230 and 245 K. The results show an obvious negative resistance effect, which indicates the magnetic nature of CrSe crystals. The findings obtained here reveal the electronic properties and magnetic properties of single-crystal CrSe.

In summary, we have successfully synthesized high-quality ultrathin nonlayered single-crystal CrSe via a facile APCVD method, for the first time. The obtained CrSe crystals exhibit triangular shapes with a lateral size of up to ≈150 µm and a thickness as low as ≈2.5 nm and a good stability in air. And a continuous CrSe film can also be obtained via precise control of the key growth parameters. Further HRTEM and SAED characterizations reveal that the CrSe triangles are single crystals and possess high crystallinity. Importantly, the magnetic characterization reveals that the CVD-grown CrSe flakes exhibit obvious ferromagnetic properties with a transition temperature close to 280 K. Additionally, the electronic properties of the CrSe crystals are further characterized by electrical transport measurements. We believe this work paves the way for controllably growing other 2D magnetic materials via a facile CVD method and may provide a new platform for investigating 2D magnetism and versatile applications in spintronics.

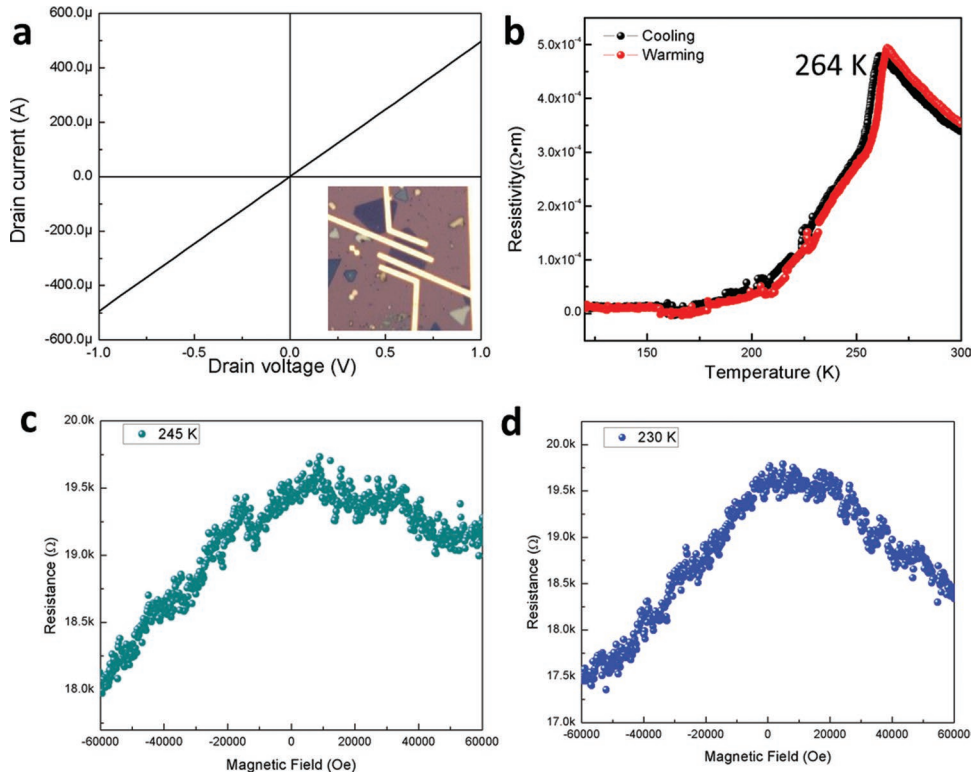

Figure 5. Electrical characterization of a CrSe crystal. a) The I_{ds}–V_{ds} curve of the CrSe device collected at room temperature. The inset shows an OM image of the fabricated four-terminal device based on transferred CrSe on SiO_2/Si. Scale bar: 10 µm. b) Temperature dependence of the resistivity of the CrSe device. c) The resistance as a function of the magnet field collected at 245 K. d) The resistance as a function of the magnet field collected at 230 K.

Experimental Section

CVD Growth of CrSe Crystals and Their Transfer: The growth of CrSe crystal was performed inside a multitemperature-zone tube furnace (Lindberg/Blue M) equipped with a 1 in. diameter quartz tube in an ambient pressure system. The CrSe crystals were synthesized by a facile APCVD technique. Selenium powder was placed in the first hot zone and mildly sublimated at ≈300 °C. $CrCl_3$ powder (Alfa Aesar, purity 99.9%) and mica substrates (Nanjing MKNANO Tech. Co., Ltd., www.mukenano.com) were successively placed inside the hot zone. A mixture of Ar and H_2 gas with flow rates of 100 and 10 sccm, respectively, was used to transport the vapor species to the downstream substrates. The growth temperature was ≈735 °C, and the growth time ranged from 10 to 30 min. As a result, ultrathin CrSe crystals were obtained on the mica substrates. The as-grown CrSe samples could be transferred intact onto an arbitrary substrate with a commonly used method. In brief, the CrSe on mica was first spin-coated with PMMA (495 K, A4, Microchem Company) via a spin coater and baked for 3 min at 180 °C. Then the CrSe supported by the PMMA film was removed from the mica substrate by tweezers under deionized water. Next, it was transferred onto a target substrate (e.g., SiO_2/Si) and dried on a heating stage. Finally, the PMMA film was removed via dissolution in acetone for ≈30 min and dried under N_2 gas. Thus, the CrSe samples were successfully transferred onto SiO_2/Si.

Characterization: The morphologies and atomic structure of the CrSe samples were characterized by OM (Olympus BX51 M), scanning electron microscopy (Hitachi SU8220), and TEM (TecnaiF20). TEM energy-dispersive X-ray spectroscopy (TEM-EDX) elemental mapping was performed by a TecnaiF20. The thickness of the obtained samples was characterized by AFM (Bruker Icon). The Raman and photoluminescence (PL) spectra were obtained from a confocal microscope-based Raman spectrometer (Renishaw InVia, 514 nm excitation laser). X-ray photoelectron spectroscopy was performed on an ESCALAB 250 Xi.

Magnetic and Electronic Measurements: The magnetic measurements were performed in different Quantum Design PPMS with vibrational sample magnetometer utility and the high magnetic fields of up to 9 T. The as-grown CrSe flakes on mica were fabricated into devices after being transferred onto SiO_2/Si. Standard electron-beam lithography processing was used to define the source/drain electrodes. Subsequently, a Cr/Au metal layer (Cr: 8 nm; Au: 60 nm) was deposited to form electrodes by thermal evaporation. Room-temperature measurements were performed with a semiconductor parameter analyzer (Keithley Model 4200-SCS). Temperature-dependent measurements of the resistivity and magnetic resistivity were performed using the different PPMS (Quantum Design) with temperatures ranging from 300 to 5 K.

Supporting Information

Supporting Information is available from the Wiley Online Library or from the author.

Acknowledgements

Y.Z. and J.C. contributed equally to this work. This work was supported by the Ministry of Science and Technology of China (Grant No. 2016YFA0200700), the National Natural Science Foundation of China (Grant Nos. 61625401, 21703047, 61474033, 61574050, and 11674072), the Strategic Priority Research Program of the Chinese Academy of Sciences (Grant No. XDA09040201), and the CAS Key Laboratory of Nanosystem and Hierarchical Fabrication. The authors also gratefully acknowledge the support of Youth Innovation Promotion Association CAS.

Conflict of Interest

The authors declare no conflict of interest.

Keywords

APCVD growth, CrSe, ferromagnetic, nonlayered material, van der Waals epitaxy

Received: January 3, 2019
Revised: March 7, 2019
Published online:

[1] H. Zeng, J. Dai, W. Yao, D. Xiao, X. Cui, *Nat. Nanotechnol.* **2012**, *7*, 490.
[2] B. Radisavljevic, A. Radenovic, J. Brivio, V. Giacometti, A. Kis, *Nat. Nanotechnol.* **2011**, *6*, 147.
[3] Q. Ji, Y. Zhang, T. Gao, Y. Zhang, D. Ma, M. Liu, Y. Chen, X. Qiao, P. Tan, M. Kan, *Nano Lett.* **2013**, *13*, 3870.
[4] V. D. Z. Am, P. Y. Huang, D. A. Chenet, T. C. Berkelbach, Y. You, G. H. Lee, T. F. Heinz, D. R. Reichman, D. A. Muller, J. C. Hone, *Nat. Mater.* **2013**, *12*, 554.
[5] H. R. Gutierrez, N. Perealopez, A. L. Elias, A. Berkdemir, B. Wang, R. Lv, F. Lopezurias, V. H. Crespi, H. Terrones, M. Terrones, *Nano Lett.* **2013**, *13*, 3447.
[6] J. Zhou, J. Lin, X. Huang, Y. Zhou, Y. Chen, J. Xia, H. Wang, Y. Xie, H. Yu, J. Lei, *Nature* **2018**, *556*, 355.
[7] H. K. Dong, S. Cho, J. H. Kim, D. H. Choe, H. J. Sung, M. Kan, H. Kang, J. Y. Hwang, S. W. Kim, H. Yang, *Nat. Phys.* **2015**, *11*, 482.
[8] E. Sohn, X. Xi, W. Y. He, S. Jiang, Z. Wang, K. Kang, J. H. Park, H. Berger, L. Forró, K. T. Law, *Nat. Mater.* **2018**, *17*, 504.
[9] M. Chhowalla, H. S. Shin, G. Eda, L. J. Li, K. P. Loh, H. Zhang, *Nat. Chem.* **2013**, *5*, 263.
[10] M. Y. Li, Y. Shi, C. C. Cheng, L. S. Lu, Y. C. Lin, H. Tang, M. L. Tsai, C. Chu, K. Wei, J. He, *Science* **2015**, *349*, 524.
[11] M. Bonilla, S. Kolekar, Y. Ma, H. C. Diaz, V. Kalappattil, R. Das, T. Eggers, H. R. Gutierrez, M. H. Phan, M. Batzill, *Nat. Nanotechnol.* **2018**, *13*, 289.
[12] V. Carteaux, F. Moussa, M. Spiesser, *Europhys. Lett. (EPL)* **1995**, *29*, 251.
[13] J. F. Dillon, H. Kamimura, J. P. Remeika, *J. Phys. Chem. Solids* **1966**, *27*, 1531.
[14] C. Gong, L. Li, Z. Li, H. Ji, A. Stern, Y. Xia, T. Cao, W. Bao, C. Wang, Y. Wang, *Nature* **2017**, *546*, 265.
[15] B. Huang, G. Clark, E. Navarromoratalla, D. R. Klein, R. Cheng, K. Seyler, D. Zhong, E. Schmidgall, M. A. Mcguire, D. Cobden, *Nature* **2017**, *546*, 270.
[16] B. Siberchicot, S. Jobic, V. Carteaux, Gressier, G. Ouvrard, *J. Phys. Chem.* **1996**, *100*, 5863.
[17] Z. Fei, B. Huang, P. Malinowski, W. Wang, T. Song, J. Sanchez, W. Yao, D. Xiao, X. Y. Zhu, A. F. May, W. Wu, D. H. Cobden, J. H. Chu, X. D. Xu, *Nat. Mater.* **2018**, *17*, 778.
[18] K. Seyler, D. Zhong, D. R. Klein, S. Gao, X. Zhang, B. Huang, E. Navarromoratalla, L. Yang, D. Cobden, M. A. Mcguire, *Nat. Phys.* **2018**, *14*, 277.
[19] Z. Wang, I. Gutiérrezlezama, N. Ubrig, M. Kroner, M. Gibertini, T. Taniguchi, K. Watanabe, A. Imamoğlu, E. Giannini, A. F. Morpurgo, *Nat. Commun.* **2018**, *9*, 2516.
[20] S. Jiang, J. Shan, K. F. Mak, *Nat. Mater.* **2018**, *17*, 406.
[21] Y. Deng, Y. Yu, Y. Song, J. Zhang, N. Z. Wang, Z. Sun, Y. Yi, Y. Z. Wu, S. Wu, J. Zhu, *Nature* **2018**, *563*, 94.
[22] Y. Zhang, H. Lu, X. Zhu, S. Tan, W. Feng, Q. Liu, W. Zhang, Q. Chen, Y. Liu, X. Luo, *Sci. Adv.* **2018**, *4*, eaao6791.
[23] D. Zhong, K. Seyler, X. Linpeng, R. Cheng, N. Sivadas, B. Huang, E. Schmidgall, T. Taniguchi, K. Watanabe, M. A. Mcguire, *Sci. Adv.* **2017**, *3*, e1603113.

[24] B. Huang, G. Clark, D. R. Klein, D. Macneill, E. Navarromoratalla, K. L. Seyler, N. Wilson, M. A. Mcguire, D. H. Cobden, D. Xiao, *Nat. Nanotechnol.* **2018**, *13*, 544.
[25] R. Cheng, Y. Wen, L. Yin, F. Wang, F. Wang, K. Liu, T. A. Shifa, J. Li, C. Jiang, Z. Wang, *Adv. Mater.* **2017**, *29*, 1703122.
[26] Q. Wang, Y. Wen, K. Cai, R. Cheng, L. Yin, Y. Zhang, J. Li, Z. Wang, F. Wang, F. Wang, *Sci. Adv.* **2018**, *4*, eaap7916.
[27] X. Li, C. W. Magnuson, A. Venugopal, R. M. Tromp, J. B. Hannon, E. M. Vogel, L. Colombo, R. S. Ruoff, *J. Am. Chem. Soc.* **2011**, *133*, 2816.
[28] K. K. Kim, A. Hsu, X. Jia, S. M. Kim, Y. Shi, M. Hofmann, D. Nezich, J. F. Rodriguezniеva, M. S. Dresselhaus, T. Palacios, *Nano Lett.* **2012**, *12*, 161.
[29] X. Ling, Y. Lee, Y. Lin, W. Fang, L. Yu, M. S. Dresselhaus, J. Kong, *Nano Lett.* **2014**, *14*, 464.
[30] A. Maignan, Y. Bréard, E. Guilmeau, F. Gascoin, *J. Appl. Phys.* **2012**, *112*, 013716.
[31] J. Dijkstra, H. H. Weitering, C. F. V. Bruggen, C. Haas, R. A. D. Groot, *J. Phys.: Condens. Matter* **1989**, *1*, 9141.
[32] K. Lukoschus, S. Kraschinski, C. Näther, W. Bensch, R. K. Kremer, *J. Solid State Chem.* **2004**, *177*, 951.
[33] J. F. Bi, M. G. Sreenivasan, K. L. Teo, T. Liew, *J. Phys. D: Appl. Phys.* **2008**, *41*, 045002.
[34] Y. Liu, C. Petrovic, *Phys. Rev. B* **2017**, *96*, 134410.
[35] S. Kobayashi, H. Ueda, D. Nishio-Hamane, C. Michioka, K. Yoshimura, *Phys. Rev. B* **2014**, *89*, 163.
[36] M. Yuzuri, K. Segi, *Phys. B—Condens. Matter* **1977**, *86*, 891.
[37] J. Yan, X. Luo, F. Chen, Q. Pei, G. Lin, Y. Han, L. Hu, P. Tong, W. H. Song, X. B. Zhu, *Appl. Phys. Lett.* **2017**, *111*, 022401.
[38] L. M. Corliss, N. Elliott, J. M. Hastings, R. L. Sass, *Phys. Rev.* **1961**, *122*, 1402.
[39] S. Polesya, S. Mankovsky, D. Benea, H. Ebert, W. Bensch, *J. Phys.: Condens. Matter* **2010**, *22*, 156002.
[40] P. Yang, X. Zou, Z. Zhang, M. Hong, J. Shi, S. Chen, J. Shu, L. Zhao, S. Jiang, X. Zhou, *Nat. Commun.* **2018**, *9*, 979.
[41] J. Shi, D. Ma, G. Han, Y. Zhang, Q. Ji, T. Gao, J. Sun, X. Song, C. Li, Y. Zhang, *ACS Nano* **2014**, *8*, 10196.
[42] Y. Zhang, Y. Zhang, Q. Ji, J. Ju, H. Yuan, J. Shi, T. Gao, D. Ma, M. Liu, Y. Chen, *ACS Nano* **2013**, *7*, 8963.
[43] Y. Zhang, L. Yin, J. Chu, T. A. Shifa, J. Xia, F. Wang, Y. Wen, X. Zhan, Z. Wang, J. He, *Adv. Mater.* **2018**, *30*, 1803665.
[44] H. Wang, X. Huang, J. Lin, J. Cui, Y. Chen, C. Zhu, F. Liu, Q. Zeng, J. Zhou, P. Yu, *Nat. Commun.* **2017**, *8*, 394.
[45] Y. Zhao, J. Qiao, Z. Yu, P. Yu, K. Xu, S. P. Lau, W. Zhou, Z. Liu, X. Wang, W. Ji, *Adv. Mater.* **2017**, *29*, 1604230.